Isothermal oxidation kinetics of nitrided Ti-6Al-4V studied by infrared emissivity

I. González de Arrieta[a], L. González-Fernández[b,c,*], E. Risueño[b,c], T. Echániz[d,e], M.J. Tello[b,e]

[a]Applied Physics II, University of the Basque Country UPV/EHU, Leioa, 48940, Spain
[b]Condensed Matter Physics, University of the Basque Country UPV/EHU, Leioa, 48940, Spain
[c]CIC Energigune, Albert Einstein 48, Miñano, Álava 01510, Spain
[d]Applied Mathematics, University of the Basque Country UPV/EHU, Bilbao, 48013, Spain
[e]Instituto de Síntesis y Estudio de Materiales, Universidad del País Vasco UPV/EHU, Apdo. 644, Bilbao 48080, Spain

Abstract

The oxidation kinetics of Ti-6Al-4V samples nitrided in forming gas ($N_2+5\%H_2$) between 520 and 805 °C is investigated using infrared emissivity measurements. Several kinetic exponents have been observed depending on temperature and time. The activation energy corresponding to the main parabolic rutile growth stage is 223 ± 10 kJ/mol. This value is significantly higher than that corresponding to TiN oxidation, which suggests that it is not the rate-limiting step. The protective role of the nitridation is attributed to the internal Ti_2N layer. The microstructural characterization reveals a reduction in the oxygen-diffusion depth compared to non-nitrided Ti-6Al-4V, and a multi-layered Al_2O_3-TiO_2 oxide.

Keywords: A: titanium, A: alloy, B: IR spectroscopy, B: XRD, B: SEM, C: high temperature corrosion

1. Introduction

The high strength-to-weight ratio and excellent biocompatibility of titanium and its alloys have been widely exploited in sectors such as aeronautics and biomedicine. In particular, the $\alpha + \beta$ Ti-6Al-4V alloy remains the world standard for these applications, traditionally accounting for the largest share of the global titanium alloy production [1, 2]. Initially developed for aerospace and aircraft components, it is now a staple of marine applications, power generation, automotive parts, sports, and medicine, with further applications expected to grow even further due to improvements in processing technology [3].

The main disadvantage of titanium alloys is its poor resistance to high-temperature corrosion and wear, which limit its working temperature range to about 400 °C and can also be troublesome in joint implants, where friction may lead to leaching of dangerous ions to the body. A number of treatments have

---

*Corresponding author
Email address: lgonzalez@cicenergigune.com (L. González-Fernández)

been attempted to improve on these surface properties, with thermal oxidation (TO) being considered one of the simplest and most cost-effective [4–7].

TO processes require good knowledge of corrosion kinetics and morphology. Moreover, these data are also essential if the working temperatures of this alloy are to be increased. However, literature data about this topic reveal a generally complex oxidation behaviour, with kinetic laws ranging from linear to cubic at different temperatures and time scales, as well as differences in activation energy and morphology [8–11].

Nitriding treatments have been known for a long time to be useful for improving the wear resistance and other tribological properties of titanium alloys [12, 13]. Among them, gas nitriding has also been suggested as a potentially effective treatment against oxidation [14–16]. However, to our knowledge, only one qualitative study of the temperature-dependent oxidation kinetics of nitrided Ti-6Al-4V has been performed [17].

This work contains a study on the oxidation kinetics and morphology of Ti-6Al-4V samples pre-nitrided in $N_2+5\%H_2$ using infrared emissivity measurements. Conventional oxidation kinetics studies rely mostly on weight-based measurement methods. Alternative techniques capable of determining oxidation kinetics include those based on optical techniques, such as emissivity measurements. This procedure takes advantage of the spontaneous thermal radiation emitted by the sample itself at the high temperatures required for oxidation. The use of alternative techniques (mainly those capable of higher sampling frequencies) is useful for reducing systematic errors and cross-validating results. The method followed in this work has been described previously in the literature [18, 19]. Studies on the evolution of the emissivity during oxidation of both titanium [20, 21] and Ti-6Al-4V [22] have been made, but the discussion of the oxidation kinetics and morphology has been scarce and qualitative. The overall purpose of this study is to evaluate the effects of nitriding in an N_2/H_2 atmosphere for the subsequent thermal oxidation of Ti-6Al-4V.

2. Experimental details

The samples used in this study were cut from the same batch of commercial Ti-6Al-4V (6.59% Al, 4.10 % V, 0.24 % Fe, 0.002 % N, 0.21 % O). The samples were ground with 80 to 320 grit SiC paper and cleaned in an acetone ultrasonic bath. The roughness of the samples was measured with a conventional roughness tester before the treatments. A range of values from 0.25 to 0.48 μm was found for the average roughness of the five samples ($R_a = 0.38 \pm 0.09$ μm). This roughness level is similar to others in the literature [15–17].

Oxidation kinetics were determined using the infrared emissivity method [18, 19]. Time-dependent emissivity measurements were carried out using the high-accuracy infrared emissometer HAIRL [23], formed by three main modules: a vacuum sample chamber, a FTIR spectrophotometer and a blackbody source for radiance calibration. The vacuum chamber allows to carry out the measurements in a controlled atmosphere. The sample temperature is measured using two bare Type K thermocouples spot-welded on the sample surface out of the area viewed by the detector. The emissivity is measured directly using the *blacksur* method [24] and the modified two-temperature calibration method [25]. All the sources of emissivity uncertainty have been analyzed for this apparatus

2

[26]. A spectral resolution of 16 cm^{-1} was chosen, with wavelength accuracy being ensured by using an FTIR spectrophotometer.

The emissivity results acquired during the oxidation process of the five samples can be employed to determine the oxidation kinetics. As the oxide scale grows, the emissivity spectra show interferential effects due to reflections at the interfaces [18, 19]. The oxide scale thickness is related to the maxima and minima position in the spectra according to the following equations:

$$d' = \frac{2m - 1}{4}\lambda \tag{1}$$

$$d' = \frac{m}{2}\lambda \tag{2}$$

where m stands for the order of the interference, λ is the wavelength of the interferential maximum (1) or minimum (2) and d' (hereafter simply d) is the apparent oxide film thickness (real thickness multiplied by the real part of the refractive index of the oxide) [19].

Eight samples were used in this study. Three samples were used to test the effects of hydrogen content in the nitridation of this alloy: one acted as a control sample, while the two others were treated at 850 °C for 2 h in 1-bar atmospheres of high-purity N_2 ($\leq$ 3 ppmv H_2O, $\leq$ 2 ppmv O_2, $\leq$ 0.5 ppmv hydrocarbons) and commercial forming gas ($N_2+5\%H_2$), respectively. Then, the five remaining samples were treated in $N_2+5\%H_2$ at 850 °C for 2 h and then isothermally oxidized at different temperatures. Measurements of the normal spectral emissivity were used as indicators of the surface state of the sample during the process, as it was observed that it is sensitive to changes in the surface [27]. After the treatment was finished, the samples were stabilized at the required temperature for oxidation, and the chamber was opened to laboratory air. The normal spectral emissivity was then measured in a continuous mode during the corrosion process.

Phase identification was carried out by X-ray diffraction (XRD) measurements in the Bragg-Brentano geometry with Cu K_α radiation and a step increment of 0.026°. The surface and cross-section morphologies and distributions of the elements were studied using a JEOL JSM-6400 scanning electron microscope (SEM) equipped for energy-dispersive X-ray spectroscopy (EDX). Images were taken at a working distance of 15 mm with backscattered electrons for compositional contrast and an accelerating voltage of 20 kV. EDX maps correspond to the distributions of the intensities of K_α lines for all components except for V, for which the K_β lines have been recorded to avoid overlap with Ti lines.

3. Results and discussion

3.1. Nitridation

Fig. 1 shows the XRD diffractograms of the first set of samples used to determine the influence of nitridation in the two atmospheres under consideration. The pattern corresponding to the untreated sample features peaks corresponding to the α and β phases. Significant differences are observed in the case of the nitrided samples, where both TiN and Ti_2N phases can be observed, with higher integrated intensities in the case of the sample nitrided in forming gas.

This could be expected due to the catalytic effect of hydrogen in nitridation, which allows a deeper penetration of nitrogen in the titanium matrix [13].

A second observation concerns the evolution in the α phase of the nitrided samples. Some of its peaks experience a noticeable shift to lower angles. This corresponds to an increase in the c/a ratio [28], which has been shown to correlate strongly to the hardness of the material [29–31]. It is thus shown that the nitriding treatment hardens the subsurface in a similar way for both atmospheres. In the case of the (002) peak at $38 - 39°$, a shoulder to the left of the main peak appears for both nitrided samples. A similar feature seems to appear in the following (101) peak at $40 - 41°$ for the forming-gas-treated sample, whereas the feature in the N_2-treated diffractogram can be better accounted for by some remaining cubic β phase (with a shortened cell parameter with respect to the untreated sample). The presence of similar shoulders has been noted in the literature [28, 32]. These minor peaks hint at an α-like phase with similar cell parameters than both the original α and the hardened α, which is sometimes tentatively described as martensite α'. Their stronger presence for the (002) peak $(38 - 39°)$ is perhaps consistent with the larger breadth of this peak for the untreated sample, which is linked to the presence of residual martensite in the original sample [33].

3.2. Oxidation kinetics

Five samples have been oxidized at temperatures from 520 °C to 805 °C. Fig. 2 shows, as an example, the interferential emissivity oscillations as a function of oxidation time for various wavelengths at 600 and 740 °C. In agreement with Eq. (1), in both cases the time needed to reach the first-order interferential maximum increases with wavelength. It is worth mentioning that the time required to observe the first maximum at 600 °C is almost two orders of magnitude higher than the one for 740 °C. These interferential patterns stop when the oxide layer is thick enough to become opaque at such wavelengths. This highlights the advantage of a wide spectral range when using optical techniques for studying oxidation kinetics, with the mid-infrared range being the one that remains semi-transparent for the longest time [34].

The time dependence of the apparent oxide thickness can be obtained directly from the interferential maxima and minima by applying Eqs. (1) and (2). Following Ref. [8], log-log plots of the growth of the oxide layer thickness with time at each temperature are shown in Fig. 3. The kinetic exponents have been calculated using the standard empirical equation:

$$d^n = kt \tag{3}$$

where d is the apparent oxide thickness, n the kinetic exponent, k the apparent rate constant and t the oxidation time.

In the case of the samples oxidized at temperatures below 700 °C (Figs. 3a-c), the oxidation process takes place with a single well-defined exponent, except for the early stages of the oxidation at 520 °C, where a transitory process of linear-parabolic nature is observed. This is consistent with a surface mode of oxidation transforming into a diffusion process once a sufficiently thick layer is formed. It is important to mention that this method is capable of detecting apparent oxide layer thicknesses of at least one-quarter of the lowest measurable wavelength. Therefore, it cannot probe the earliest stages of the oxidation below

such thicknesses, and thus it cannot discard a similar transitory stage for the other oxidation temperatures (such as the one hinted at in Fig. 3c). These results show a clear temperature dependence of the kinetic exponent, decreasing clearly from near-cubic (2.58) to near-parabolic (1.86) to linear-parabolic (1.69). Despite this evolution, the overall kinetics can still be described within the same framework (corresponding to the diffusive growth of a rutile layer), similarly to the results reported in Ref. [10].

Figure 3 also shows that, in the case of temperatures above 700 °C, three processes with similar structure can be observed. The oxidation follows firstly a clear parabolic behaviour which is interrupted by a temporary diversion into cubic kinetics, before proceeding on to the final stage, which is either parabolic again (740 °C, Fig. 3d) or linear (805 °C, Fig. 3e). This is consistent with the observed spallation in the case of the sample oxidized at 805 °C, and also with literature data, which sets 800 °C as the limit of parabolic kinetics [8]. It should be noted that the oxidation process shown in this article at 805 °C does feature higher-than-linear kinetics for the first three hours of oxidation ($n = 1.93$), which suggests a regular diffusion-limited oxidation process. Other works have also reported such type of kinetics, with spallation occurring only above a certain time threshold [8]. This indicates that the linear kinetics around 800 °C are not due to an intrinsically defective oxide layer but to a susceptibility to crack and the inability of the oxide layer to recover at high temperatures. Overall, the observed kinetics for the oxide layer growth is complex but consistent with the better-established cases of non-nitrided Ti-6Al-4V and Ti.

3.3. Activation energy

The main parabolic or quasi-parabolic (in the case of 520 °C and 665 °C) stage of each of the five temperatures in Fig. 3, which are assumed to correspond to the growth of the main rutile layer, have been fitted to the following formula [35]:

$$(d - d_0)^2 = k_p(t - t_0) \tag{4}$$

where k_p corresponds to the parabolic constant, d_0 is the initial thickness, and t_0 is the duration of the faster transient oxidation stage.

An activation energy of 223 ± 10 kJ/mol has been found, as shown in Fig. 4. This energy is similar to that obtained for pure titanium [9] and higher than some reported values for Ti-6Al-4V [10], but much lower than those reported for the corresponding parabolic kinetics in Ti-6Al-4V and Ti-Al alloys (~ 270 kJ/mol) [8, 9, 11]. It should be mentioned that the activation energies obtained through weight-gain measurements account for the total oxygen uptake (i.e., oxide layer growth plus oxygen diffusion), whereas those based in thickness measurements account only for the growth of the oxide layer. Out of the aforementioned works, only Ref. [10] reports a separate activation energy for oxide layer growth in air for Ti-6Al-4V (147 kJ/mol), which is significantly lower than the value reported in this work. The reported value is therefore much closer to the self-diffusion activation energy of rutile (251 kJ/mol) [36]. Finally, the observed activation energy is also significantly higher than the values reported for TiN (110-136 kJ/mol), which suggests that the oxidation of this phase is not the rate-limiting step in this case [37]. On the contrary, Ti_2N is known to be a better barrier against diffusion [38, 39], although no activation energy has been

found for the oxidation of this compound in air. Interestingly, it has been established that oxide growth on top of nitride phases proceeds by outward titanium diffusion [14], contrary to the inward oxygen diffusion that is mostly responsible for the oxidation of pure titanium [8]. This may represent a fundamental difference in the oxidation process, which remains throughout the rutile growth stage. This may be due to the internal Ti_2N layer controlling the nature of the diffusing species.

It has been claimed that nitridation at high temperatures leads to the same oxidation rates for pure titanium and Ti-6Al-4V [14]. It has also been stated that rutile formed in the presence of nitrogen features a larger unit cell volume than pure TiO_2, due to the substitution of O ions by trivalent N ions. The presence of defects alters the diffusion paths available for O, and could, therefore, affect the activation energy [40]. Thus, a tentative hypothesis may involve a negation of the beneficial effects of the Al content when the concentration of N ions in rutile is so large. Moreover, the concentration of Al in the surface is reduced due to its low solubility in titanium nitrides and the observed segregation in nitrided Ti-6Al-4V [15]. However, the absence of more data on the specific activation energy associated with the growth of the oxide layer itself makes comparisons to regular Ti-6Al-4V difficult. To our knowledge, no activation energy data on nitrided Ti-6Al-4V is available in the literature, as most literature on the topic has focused on the microstructure of the nitrided alloy, and not on the kinetics of the process. Even when kinetics have been studied [14, 17], there have been no reports on activation energy values.

3.4. XRD characterization of the oxidized samples

Fig. 5 shows the XRD patterns corresponding to samples oxidized at low, medium and high temperatures. Rutile and alumina are the only oxidation products seen, while a still significant Ti_2N presence can also be observed for the sample oxidized at 520 °C. This residual presence, together with the quasi-cubic kinetics, suggests that the formation of nitrides is effective against corrosion at relatively low temperatures. It should be noted that no anatase TiO_2 has been found for any sample, in contradiction with a number of studies on non-nitrided Ti-6Al-4V [6, 7, 11, 22, 29]. As anatase is less protective than rutile against certain modes of corrosion (e.g., by reducing acids) [7], its absence after nitriding could be positive for the development of this method of protection. On the other hand, improved osteogenic activities have been suggested for mixed anatase-rutile layers in pure Ti [41]. Oxidation of nitrided samples in the literature was performed at temperatures higher than those where anatase is expected to form, so no comparison is possible. Nevertheless, it has been stated that the amount of anatase formed at 500 °C for short oxidation times decreases with time at the same time that the amount of Ti(O) phase grows [6].

In order to focus on the evolution of the α phase (in connection with Section 3.1), X-ray diffractograms of the samples oxidized at the lowest temperatures are shown in Fig. 6. Interestingly, peaks corresponding to Ti_2N (but not TiN) are observed in the diffractogram corresponding to the sample oxidized at 520 °C, which indicates that this phase remains during the rutile-forming stages. Besides, a decrease in the amount of α phase is noted, together with a surge in a new phase with the same space group and similar lattice constants. This α-like phase, which was already observed in Section 3.1, has not been conclusively identified. Similar shoulders have been reported in the literature, mostly linked

to the *hcp* martensite α' phase [28, 32]. Precipitation of α_2-Ti$_3$Al in the subsurface of oxidized Ti-6Al-4V has also been described in [42]. Other complex subsurface microstructures have been reported, for example, for oxidized Ti-6Al-4V-1B, in which the presence of an additional element (boron) stimulates the precipitation of new phases [43]. The information shown in this angular range is supported by extra peaks in other ranges, but no ultimate conclusion can be inferred from the data to suggest a definitive indexation. In any case, the structure of the α phase is not critical for the interpretation of this work.

Similar to the analysis in Section 3.1, the angular shift of the α peaks can be correlated with an increase in the c/a ratio. A similar shoulder to the one found for the nitrided samples can be seen for the sample oxidized at the lowest temperature (520 °C), whereas the shape of the diagram for the sample oxidized at 600 °C hints at a double peak feature for the (002) peak at 38°. Finally, multiple α-like phases are no longer observed for the sample oxidized at 665 °C. Interestingly, even the (100) peak at $35 - 36°$ shifts to lower angles in this case. This corresponds to a change in all the lattice parameters, not only the c/a ratio, as this peak depends only on the a parameter. It can be seen that oxidation at low temperatures does not induce significant changes to the subsurface of the alloy with respect to nitridation, but stronger effects are observed at higher temperatures.

3.5. SEM characterization of oxidized samples

Surface SEM images for samples oxidized at low, medium and high temperatures are shown in Fig. 7. The sample oxidized at 520 °C shows the texture of the underlying substrate, with very little oxidation. Small nucleation sites with sizes much lower than 1 μm can be observed. As temperature rises, the formation of granular oxide particles can be observed, which cover the surface completely, hiding the substrate morphology. For the oxidation at 665 °C (Fig. 7b), the particle size distribution is relatively homogeneous at 0.5-1.5 μm, whereas for the highest temperature (Fig. 7c) a more irregular morphology is observed, with significant protuberances and more heterogeneous particle sizes (ranging from 0.25 to 2-3 μm).

The surface morphology of all samples is very similar to that in Ref. [14], where it was shown that nitridation at high temperatures led to smoother oxidized surfaces with finer and better-crystallized grains than in the non-nitrided case, independent of the underlying microstructure. In particular, the formation of coarse nodules is avoided by nitridation. This may be of interest for biomedical applications, as sharper and more homogeneous surface morphologies show improved wettability [41].

A cross-sectional SEM image of the sample oxidized at 805 °C is shown in Fig. 8. As seen in other references for nitrided Ti-6Al-4V [14], there is a relatively large amount of β phase in the subsurface of the alloy, contrary to the more established case of regular Ti-6Al-4V [8–11]. Whereas the concentration of subsurface β phase is lower than in the bulk of the material, it is still present, and so no α case can be said to be formed for this alloy. Despite the significant evolution of the α phase evidenced by XRD, there is no formation of a β-less case several μm deep. This effect of nitridation has been corroborated in other works [14]. Nevertheless, it should be noted that, also because of nitridation, the hardening effect shown in Fig. 6 is taking place in a much thinner diffusion zone, when compared with the standard results of oxidation in air. This could

be advantageous for improving the mechanical properties of the alloy. Hardness tests have not been attempted due to the small size of the diffusion layer and the significant presence of β grains near the surface, which makes the hardness inhomogeneous at the μm range [14].

In order to discern the origin of the cubic oxidation regimes at such temperatures, a compositional EDX map of the oxide layer is shown in Fig. 9 (a different location is shown in the Supplementary Material). It can be easily seen that the oxidation product is not a uniform layer, but consists of a top alumina layer, and two thick rutile sublayers separated by a much thinner alumina layer located below a lateral crack. Such morphologies can be observed in some reported micrographs of oxidized Ti-6Al-4V, although not as the focus of the study [11]. Based on the observation of a periodic stacking of rutile and alumina layers, a model was formulated for the oxidation of Ti-6Al-4V [8], in which these bilayers grow again after each crack of the previous layer. The formation of alumina between two rutile growth stages is consistent with the cubic rates (or higher) found for the samples oxidized at the highest temperatures (Figs. 3d-e). This is also in accordance with other experimental results, which indicate that the growth of Al_2O_3 in alloys generally follows such kind of exponents [44].

4. Conclusions

The effects of nitriding in forming gas in the oxidation kinetics and morphology of Ti-6Al-4V have been studied. It is shown that the hydrogen content allows for more effective formation of nitrides in this alloy. The presence of such layers is advantageous, leading to finer surface morphologies, thinner diffusion layers, absence of anatase and mostly protective oxide layers. The kinetics of the oxidation process has been discussed in terms of the mechanisms behind them. The samples oxidized at temperatures below 700 °C feature a quasi-parabolic behaviour, with a rate exponent which steadily decreases with temperature. In the case of the two highest temperatures, a more complex behaviour has been observed, due to the cracking of the rutile layer and the formation of an intermediate alumina layer. An activation energy of 223 ± 10 kJ/mol has been found for the rutile forming stages. Comparison of this value to literature data for non-nitrided Ti-6Al-4V is difficult, as reported values usually correspond to the total oxygen intake, instead of the oxide layer growth.

Data statement

Data will be made available on request.

References

[1] R. Boyer, An overview on the use of titanium in the aerospace industry, Materials Science and Engineering: A 213 (1) (1996) 103 – 114, international Symposium on Metallurgy and Technology of Titanium Alloys. `doi:10.1016/0921-5093(96)10233-1`.

[2] C. Cui, B. M. Hu, L. Zhao, S. Liu, Titanium alloy production technology, market prospects and industry development, Materials & Design 32 (2011) 1684–1691. `doi:10.1016/j.matdes.2010.09.011`.

[3] S. Liu, Y. C. Shin, Additive manufacturing of Ti6Al4V alloy: A review, Mater. Des. 164 (2019) 107552. `doi:10.1016/j.matdes.2018.107552`.

[4] N. Lin, R. Xie, J. Zou, J. Qin, Y. Wang, S. Yuan, D. Li, L. Zhao, L. Zhang, Z. Wang, et al., Surface damage mitigation of titanium and its alloys via thermal oxidation: A brief review, Reviews on Advanced Materials Science 58 (1) (2019) 132–146. `doi:10.1515/rams-2019-0012`.

[5] C. A. R. Maestro, A. H. S. Bueno, A. M. de Sousa Malafaia, Cyclic thermal oxidation evaluation to improve Ti6Al4V surface in applications as biomaterial, Journal of Materials Engineering and Performance 28 (8) (2019) 4991–4997. `doi:10.1007/s11665-019-04220-x`.

[6] S. Kumar, T. S. Narayanan, S. G. S. Raman, S. Seshadri, Thermal oxidation of Ti6Al4V alloy: Microstructural and electrochemical characterization, Mater. Chem. Phys. 119 (1) (2010) 337 – 346. `doi:10.1016/j.matchemphys.2009.09.007`.

[7] H. Guleryuz, H. Cimenoglu, Effect of thermal oxidation on corrosion and corrosion-wear behaviour of a Ti-6Al-4V alloy, Biomaterials 25 (16) (2004) 3325 – 3333. `doi:10.1016/j.biomaterials.2003.10.009`.

[8] H. Du, P. Datta, D. Lewis, J. Burnell-Gray, Air oxidation behaviour of Ti-6Al-4V alloy between 650 and 850 °C, Corros. Sci. 36 (4) (1994) 631 – 642. `doi:10.1016/0010-938X(94)90069-8`.

[9] A. Chaze, C. Coddet, Influence of aluminium on the oxidation of titanium between 550 and 750 °C, J. Less-Common Met. 157 (1) (1990) 55 – 70. `doi:10.1016/0022-5088(90)90406-A`.

[10] S. Frangini, A. Mignone, F. de Riccardis, Various aspects of the air oxidation behaviour of a Ti6Al4V alloy at temperatures in the range $600 - 700$ °C, J. Mater. Sci. 29 (3) (1994) 714–720. `doi:10.1007/BF00445984`.

[11] H. Guleryuz, H. Cimenoglu, Oxidation of Ti-6Al-4V alloy, J. Alloy. Compd. 472 (1) (2009) 241 – 246. `doi:10.1016/j.jallcom.2008.04.024`.

[12] T. Bell, H. W. Bergmann, J. Lanagan, P. H. Morton, A. M. Staines, Surface engineering of titanium with nitrogen, Surf. Eng. 2 (2) (1986) 133–143. `doi:10.1179/sur.1986.2.2.133`.

[13] H. J. Spies, Second Lakhtin memorial lecture, Met. Sci. Heat Treat. 42 (5) (2000) 161–173. `doi:10.1007/BF02469845`.

[14] P. Pérez, Influence of nitriding on the oxidation behaviour of titanium alloys at 700 °C, Surf. Coat. Technol. 191 (2) (2005) 293 – 302. `doi:10.1016/j.surfcoat.2004.04.066`.

[15] D. Lee, I. Pohrelyuk, O. Yaskiv, J. Lee, Gas nitriding and subsequent oxidation of Ti-6Al-4V alloys, Nanoscale Res. Lett. 7 (2012) 21. `doi:10.1186/1556-276X-7-21`.

[16] D. B. Lee, W. A. Abro, K. S. Lee, M. A. Abro, I. Pohrelyuk, O. Yaskiv, Gas nitriding and oxidation of Ti-6Al-4V alloy, in: Defect and Diffusion Forum, Vol. 382, Trans Tech Publ, 2018, pp. 155–159. `doi:10.4028/www.scientific.net/DDF.382.155`.

[17] D. B. Lee, M. J. Kim, L. Chen, S. H. Bak, O. Yaskiv, I. Pohrelyuk, V. Fedirko, Oxidation of nitride layers formed on Ti-6Al-4V alloys by gas nitriding, Met. Mater. Int. 17 (3) (2011) 471–477. `doi:10.1007/s12540-011-0627-9`.

[18] L. del Campo, R. B. Pérez-Sáez, M. J. Tello, Iron oxidation kinetics study by using infrared spectral emissivity measurements below 570 °C, Corros. Sci. 50 (1) (2008) 194 – 199. `doi:10.1016/j.corsci.2007.05.029`.

[19] L. del Campo, R. B. Pérez-Sáez, L. González-Fernández, M. J. Tello, Kinetics inversion in isothermal oxidation of uncoated WC-based carbides between 450 and 800 °C, Corros. Sci. 51 (4) (2009) 707 – 712. `doi:10.1016/j.corsci.2008.12.022`.

[20] G. Neuer, F. Güntert, Insitu measurements of layer thickness during oxidation of titanium, Thermochim. Acta 133 (1988) 299 – 304. `doi:10.1016/0040-6031(88)87173-9`.

[21] F. Zhang, K. Yu, K. Zhang, Y. Liu, Y. Zhao, Y. Liu, Infrared spectral emissivity property of pure titanium in the 473-1035 K temperature range, Appl. Spectrosc. 70 (10) (2016) 1717–1725. `doi:10.1177/0003702816644757`.

[22] L. Li, K. Yu, K. Zhang, Y. Liu, Study of Ti-6Al-4V alloy spectral emissivity characteristics during thermal oxidation process, Int. J. Heat Mass Tran. 101 (2016) 699 – 706. `doi:10.1016/j.ijheatmasstransfer.2016.05.069`.

[23] L. del Campo, R. B. Pérez-Sáez, X. Esquisabel, I. Fernández, M. J. Tello, New experimental device for infrared spectral directional emissivity measurements in a controlled environment, Rev. Sci. Instrum. 77 (2006) 113111. `doi:10.1063/1.2393157`.

[24] R. B. Pérez-Sáez, L. Del Campo, M. J. Tello, Analysis of the accuracy of methods for the direct measurement of emissivity, International Journal of Thermophysics 29 (3) (2008) 1141–1155.

[25] L. González-Fernández, R. B. Pérez-Sáez, L. del Campo, M. J. Tello, Analysis of calibration methods for direct emissivity measurements, Applied Optics 49 (14) (2010) 2728–2735.

[26] L. del Campo, R. B. Pérez-Sáez, L. González-Fernández, M. J. Tello, Combined standard uncertainty in direct emissivity measurements, Journal of Applied Physics 107 (11) (2010) 113510.

[27] L. González-Fernández, E. Risueño, R. B. Pérez-Sáez, M. J. Tello, Infrared normal spectral emissivity of Ti-6Al-4V alloy in the 500-1150 K temperature range, J. Alloy. Compd. 541 (2012) 144 – 149. `doi:10.1016/j.jallcom.2012.06.117`.

[28] S. Malinov, W. Sha, Z. Guo, C. Tang, A. Long, Synchrotron X-ray diffraction study of the phase transformations in titanium alloys, Materials Characterization 48 (4) (2002) 279–295.

[29] A. Ashrafizadeh, F. Ashrafizadeh, Structural features and corrosion analysis of thermally oxidized titanium, J. Alloy. Compd. 480 (2) (2009) 849 – 852. `doi:10.1016/j.jallcom.2009.02.079`.

[30] F. Borgioli, E. Galvanetto, A. Fossati, G. Pradelli, Glow-discharge and furnace treatments of Ti-6Al-4V, Surf. Coat. Technol. 184 (2) (2004) 255 – 262. `doi:10.1016/j.surfcoat.2003.10.004`.

[31] W. Yan, X. X. Wang, Surface hardening of titanium by thermal oxidation, J. Mater. Sci. 39 (16) (2004) 5583–5585. `doi:10.1023/B:JMSC.0000039294.73283.c8`.

[32] K. Sofinowski, M. Šmíd, I. Kuběna, S. Vivès, N. Casati, S. Godet, H. V. Swygenhoven, In situ characterization of a high work hardening Ti-6Al-4V prepared by electron beam melting, Acta Materialia 179 (2019) 224 – 236. `doi:10.1016/j.actamat.2019.08.037`.

[33] S. C. Lima, R. Hinrichs, M. A. Z. Vasconcellos, The influence of nitrogen to hydrogen ratio and temperature on thickness and phase composition in plasma nitrided Ti-6Al-4V, Matéria (Rio de Janeiro) 24 (1). `doi:10.1590/s1517-707620190001.0607`.

[34] I. González de Arrieta, T. Echániz, J. M. Olmos, R. Fuente, I. Urcelay-Olabarría, J. M. Igartua, M. J. Tello, G. A. López, Evolution of the infrared emissivity of Ni during thermal oxidation until oxide layer opacity, Infared Phys. Techn. 97 (2019) 270 – 276. `doi:10.1016/j.infrared.2019.01.002`.

[35] B. Pieraggi, Calculations of parabolic reaction rate constants, Oxidation of Metals 27 (3) (1987) 177–185. `doi:10.1007/BF00667057`.

[36] D. J. Young, High temperature oxidation and corrosion of metals, Vol. 1, Elsevier, 2008.

[37] H.-Y. Chen, F.-H. Lu, Oxidation behavior of titanium nitride films, J. Vac. Sci. Technol. A 23 (4) (2005) 1006–1009. `doi:10.1116/1.1914815`.

[38] I. Abdallah, C. Dupressoire, L. Laffont, D. Monceau, A. V. Put, STEM-EELS identification of TiO_XN_Y, TiN, Ti_2N and O, N dissolution in the Ti2642S alloy oxidized in synthetic air at 650 °C, Corrosion Science 153 (2019) 191 – 199. `doi:10.1016/j.corsci.2019.03.037`.

[39] I. Pohrelyuk, O. Tkachuk, R. Proskurnyak, Effect of oxidation of nitride coatings on corrosion properties of Ti-6Al-4V alloy in 0.9% NaCl at 40 °C, Open Chemistry 12 (2) (2014) 260–265.

[40] S. A. Borbunov, N. V. Morolev, V. I. Tikhomirov, The role of nitrogen in the oxidation of titanium in air at elevated temperatures, Sov. Mater. Sci. 2 (2) (1967) 145–147. `doi:10.1007/BF00716209`.

[41] G. Wang, J. Li, K. Lv, W. Zhang, X. Ding, G. Yang, X. Liu, X. Jiang, Surface thermal oxidation on titanium implants to enhance osteogenic activity and in vivo osseointegration, Sci. Rep. 6 (2016) 31769. `doi:10.1038/srep31769`.

[42] P. Bagot, A. Radecka, A. Magyar, Y. Gong, D. Bell, G. Smith, M. Moody, D. Dye, D. Rugg, The effect of oxidation on the subsurface microstructure of a Ti-6Al-4V alloy, Scripta Materialia 148 (2018) 24 – 28. `doi:10.1016/j.scriptamat.2018.01.015`.

[43] D. Brice, P. Samimi, I. Ghamarian, Y. Liu, R. Brice, R. Reidy, J. Cotton, M. Kaufman, P. Collins, Oxidation behavior and microstructural decomposition of Ti-6Al-4V and Ti-6Al-4V-1B sheet, Corrosion Science 112 (2016) 338 – 346. `doi:10.1016/j.corsci.2016.07.032`.

[44] D. J. Tallman, B. Anasori, M. W. Barsoum, A critical review of the oxidation of Ti_2AlC, Ti_3AlC_2 and Cr_2AlC in air, Mater. Res. Lett. 1 (3) (2013) 115–125. `doi:10.1080/21663831.2013.806364`.
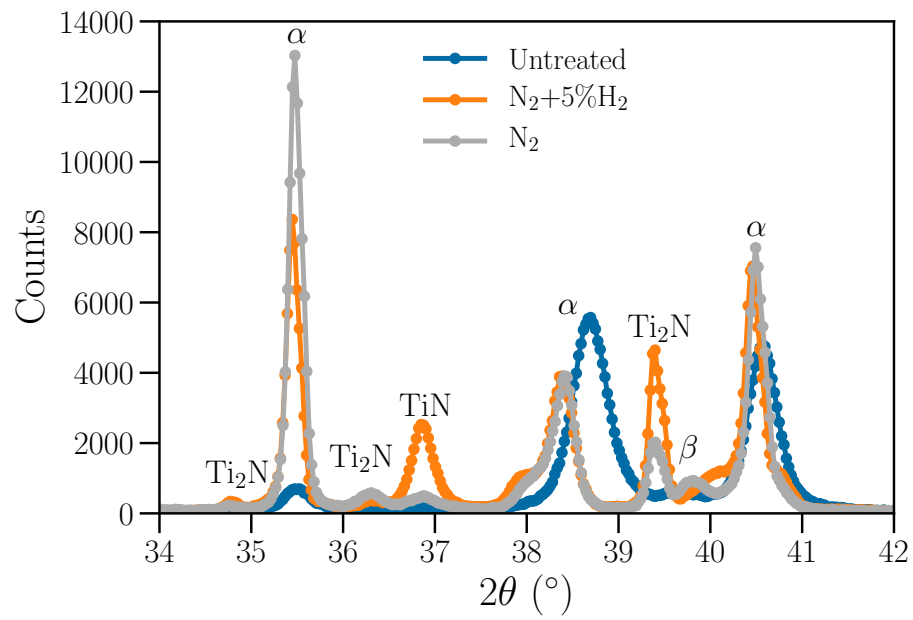
Figure 1: XRD diffractograms of the untreated sample and those treated in N_2+5%H_2 and N_2.
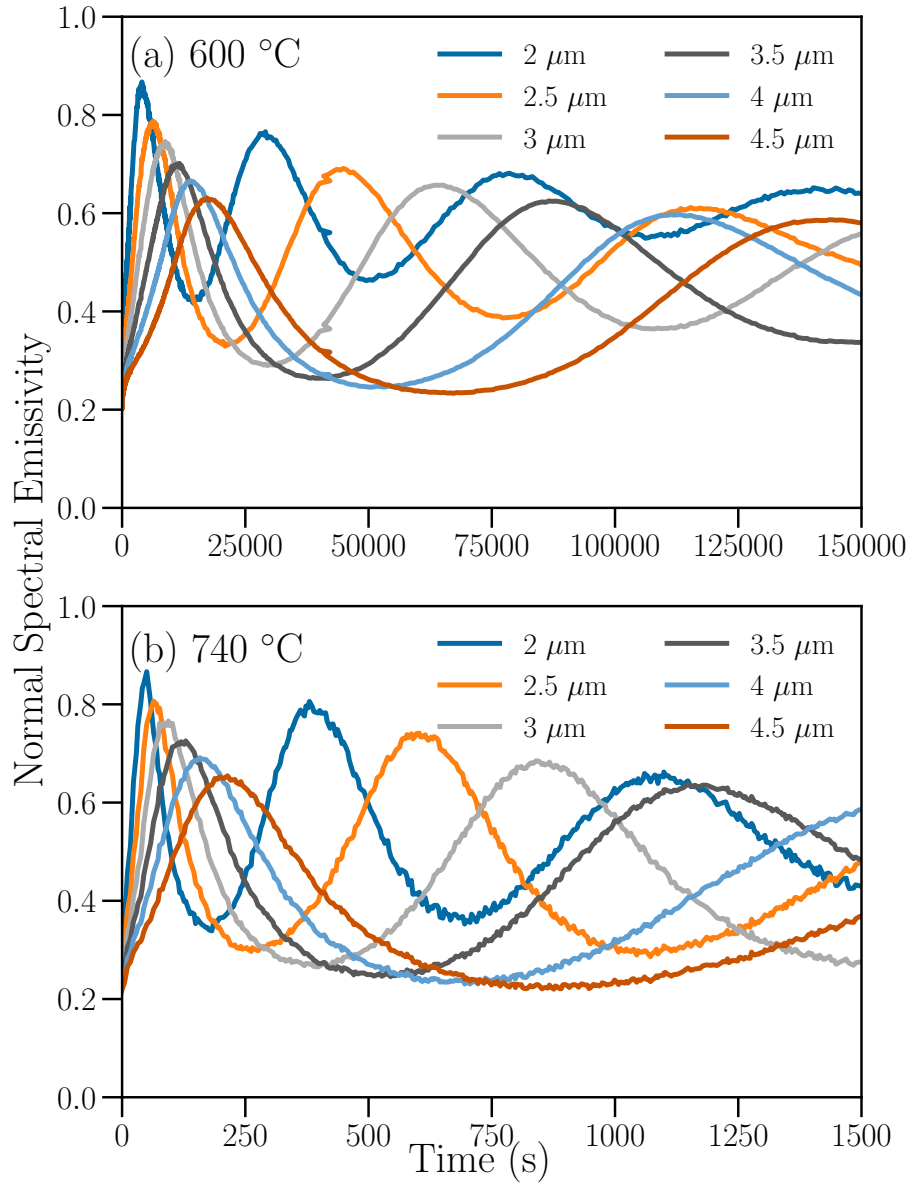
Figure 2: Temporal evolution of the normal spectral emissivity of Ti-6Al-4V at (a) 600 °C and (b) 740 °C.
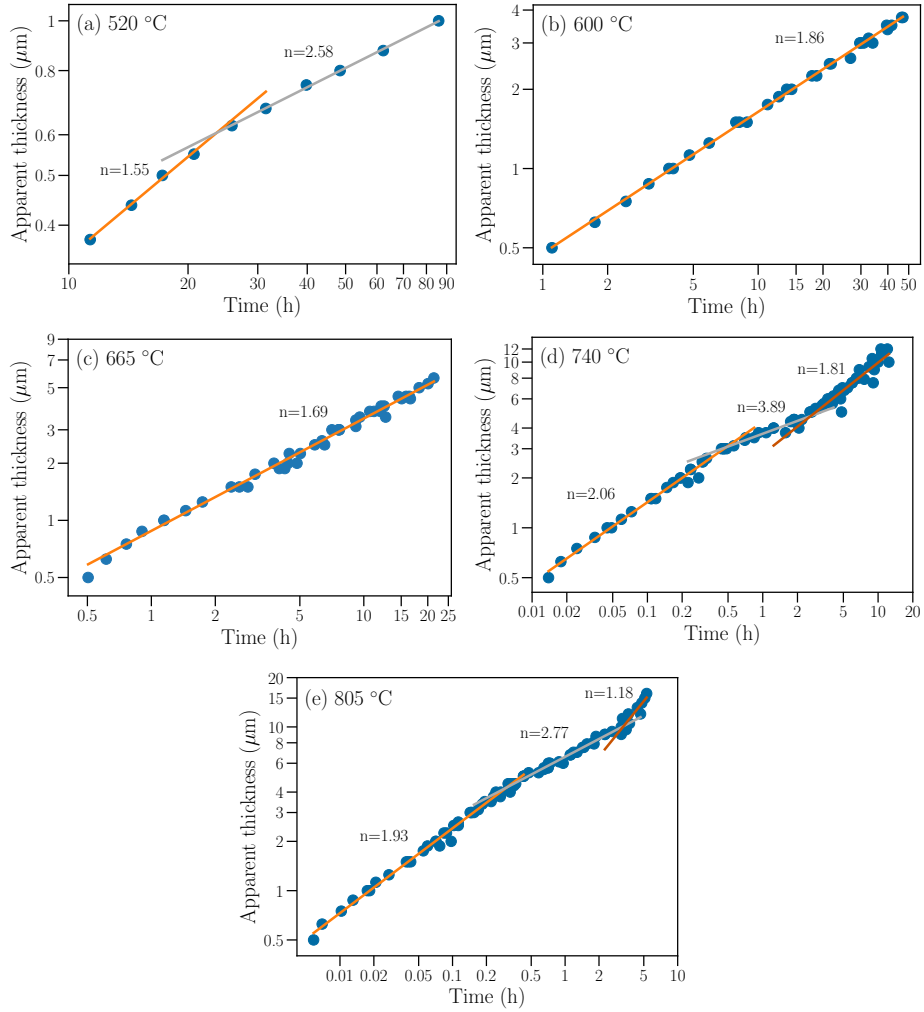
Figure 3: Growth of the oxide layer apparent thickness with time at different oxidation temperatures. Kinetic exponents obtained by fitting to Eq. (3) are shown for each distinct oxidation stage.
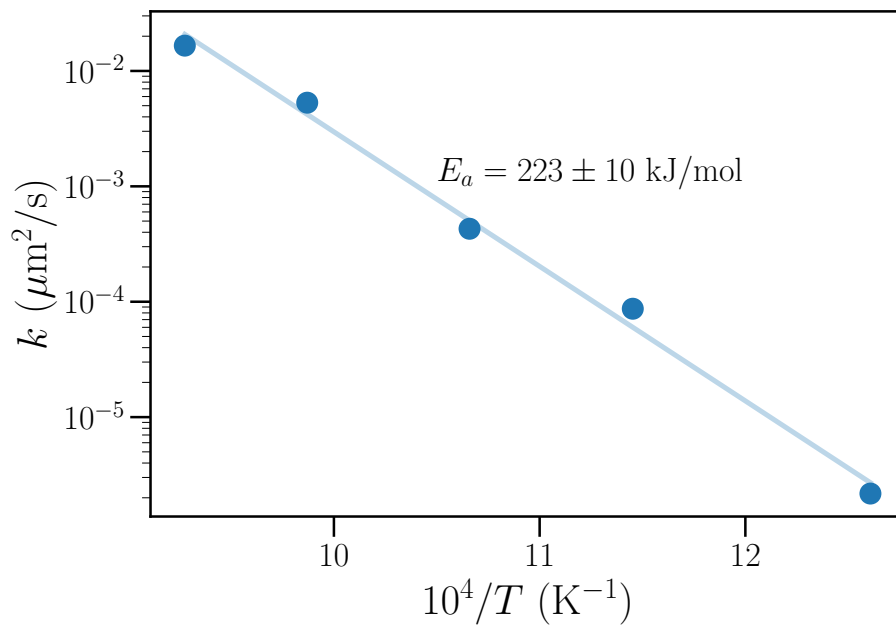
Figure 4: Arrhenius plot of the rutile-forming parabolic oxidation stages obtained by fitting the quasi-parabolic regions to Eq. 4. Activation energy: 223 ± 10 kJ/mol.
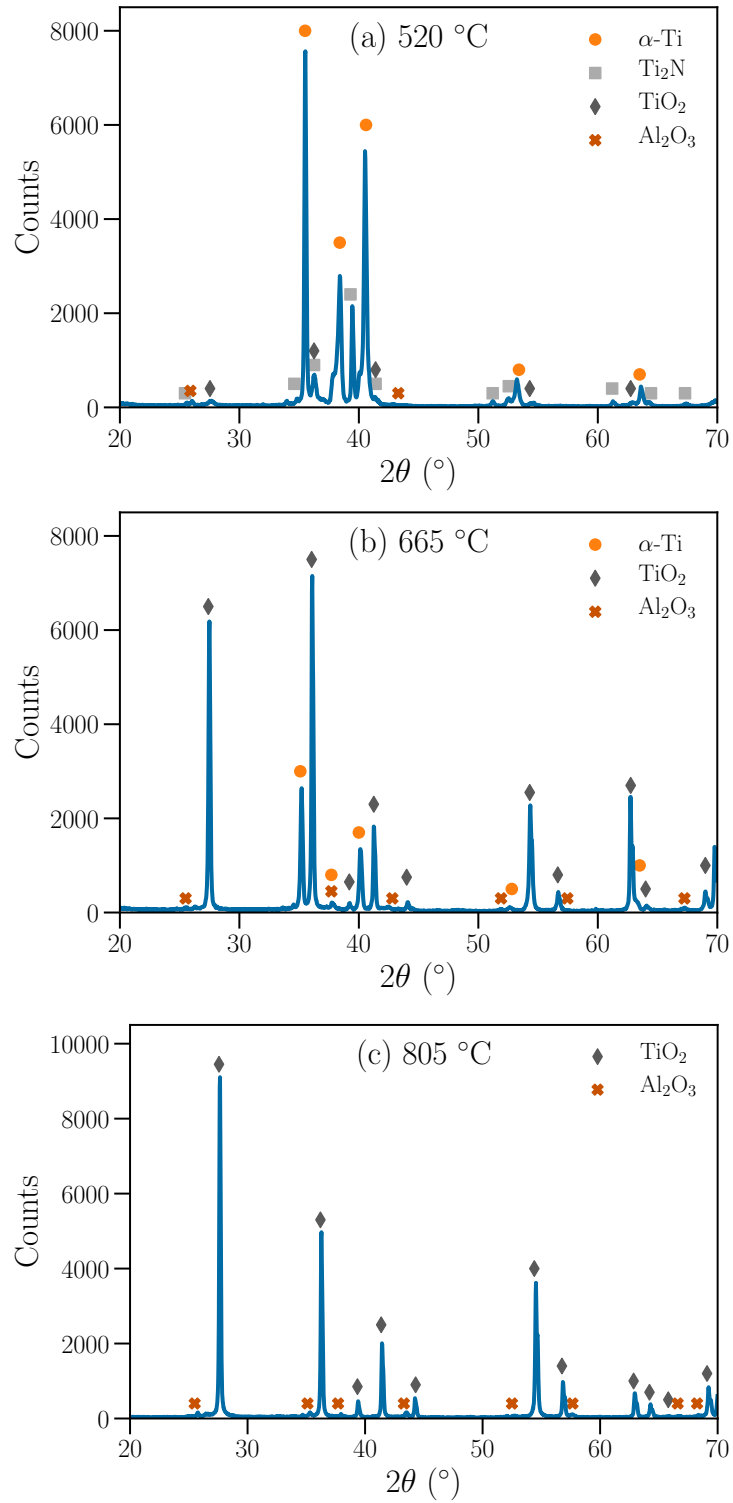
Figure 5: X-ray diffractograms for samples oxidized at (a) 520 °C, (b) 665 °C, and (c) oxide detached from the sample oxidized at 805 °C.
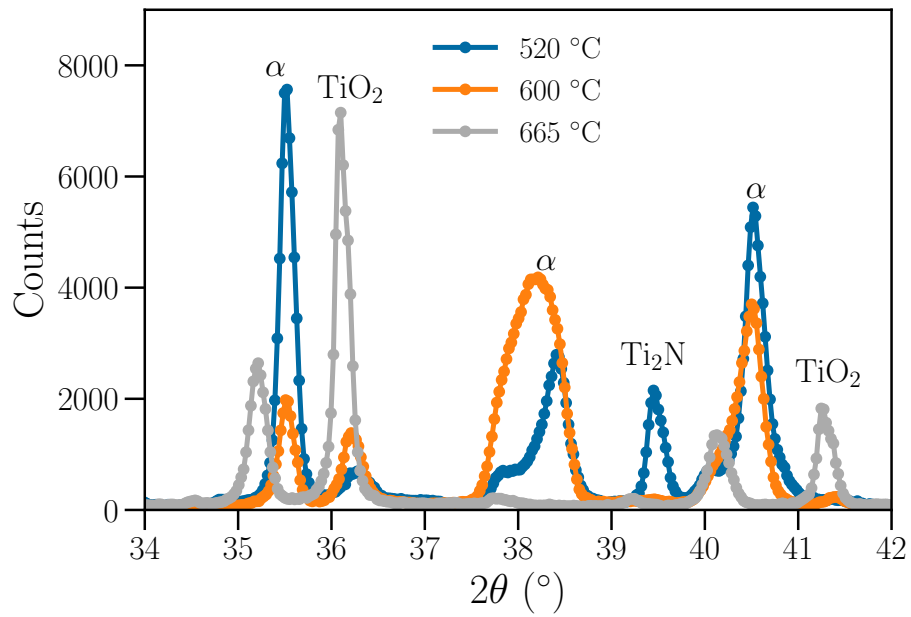
Figure 6: Close-up X-ray diffractograms of the three samples oxidized at lower temperatures.

(a) 520 °C.

(b) 665 °C.

(c) 805 °C.
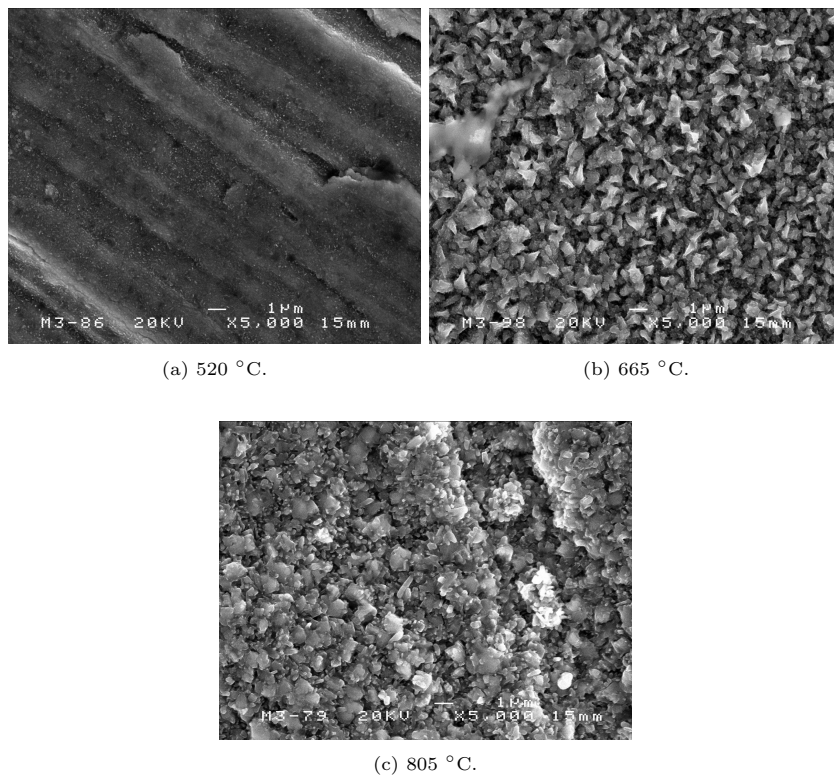
Figure 7: Surface SEM image of the oxide layer morphology at different temperatures.
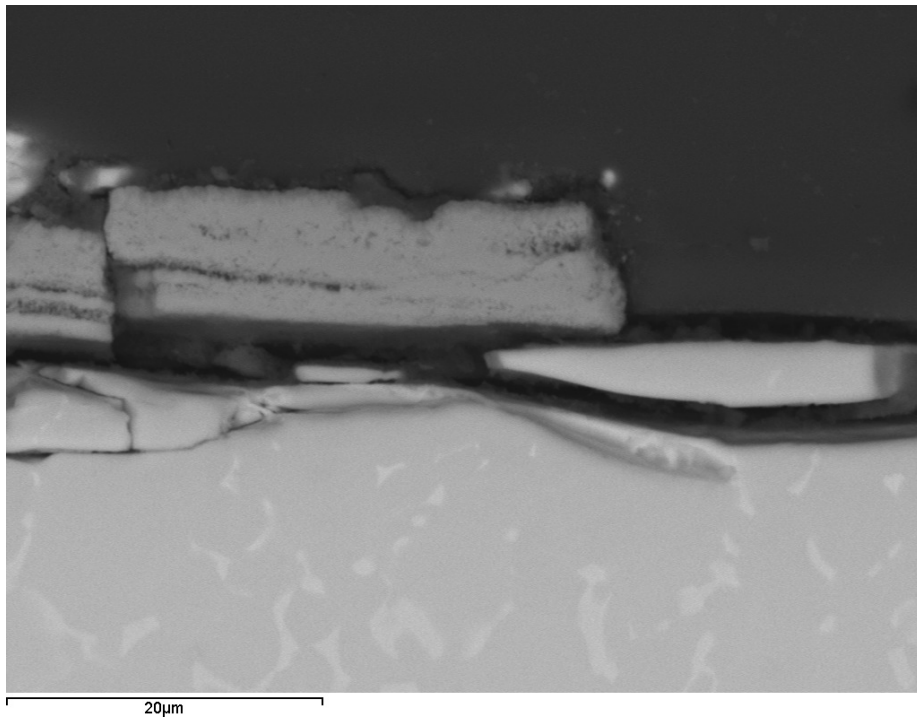
Figure 8: Large-area cross-sectional SEM image of the sample oxidized at 805 °C. The presence of β grains (light colour) near the surface is observed.
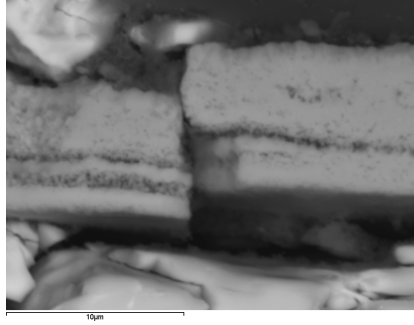
(a) Cross-sectional SEM image of the oxide layer.
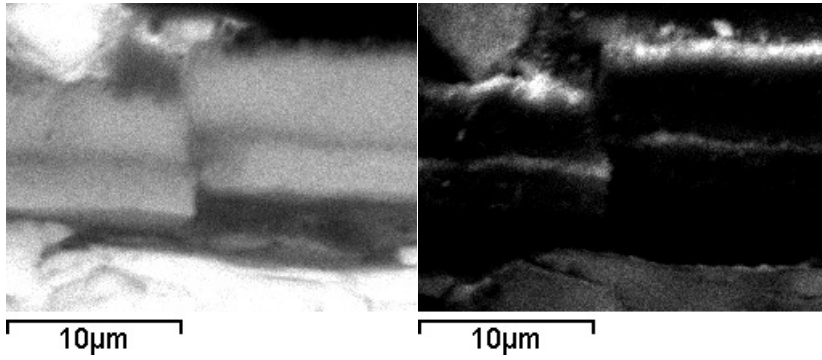
(b) EDX spectrum of Ti.

(c) EDX spectrum of Al.
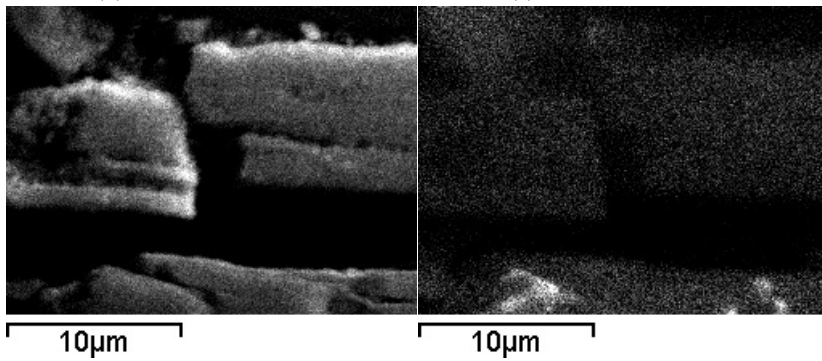
(d) EDX spectrum of O.

(e) EDX spectrum of V

Figure 9: Cross-sectional SEM image and compositional EDX maps of the the substrate-oxide layer interface.
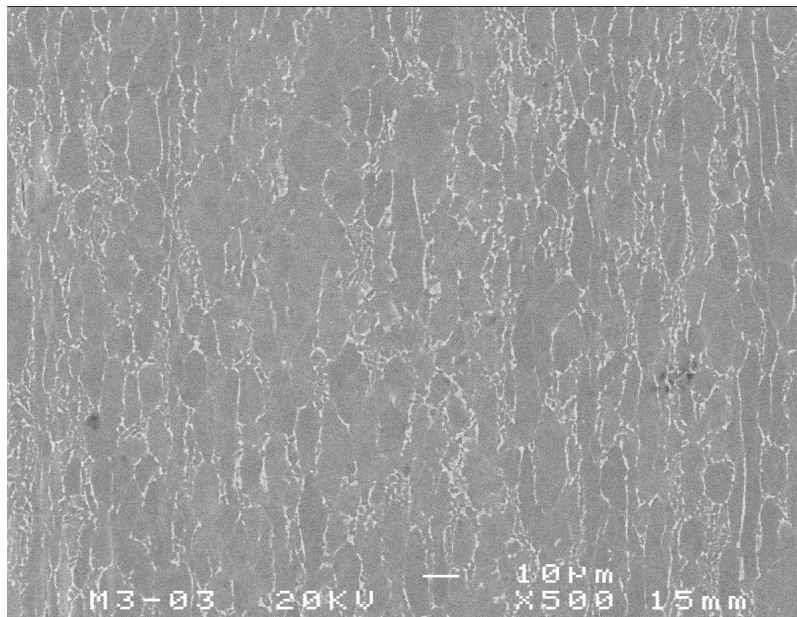
Supplementary material

Fig. S1. Bulk SEM micrograph of the untreated sample.
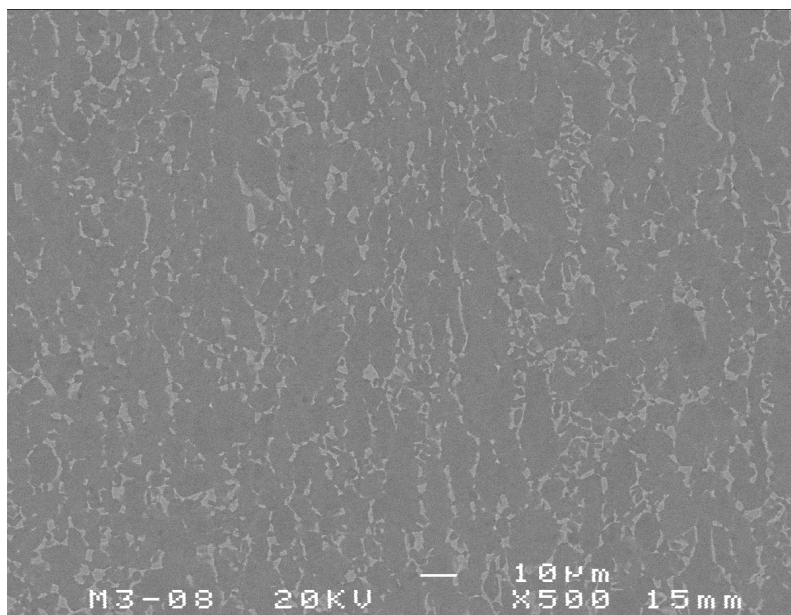

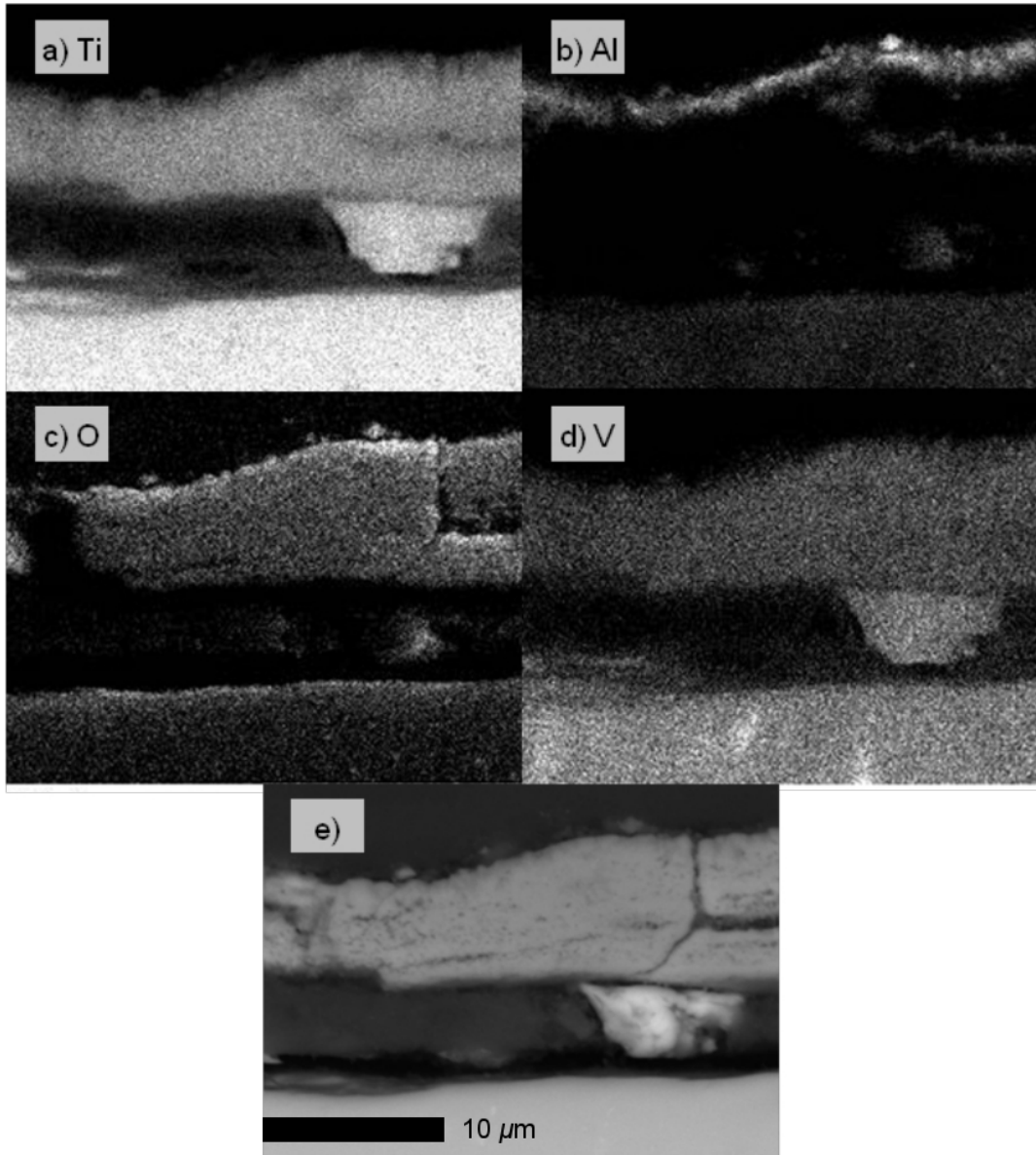Fig. S2. Bulk SEM micrograph of the sample oxidized at 520 ºC.

Fig. S3. Cross-sectional SEM micrograph and EDX compositional maps of the oxide layer on top of the sample oxidized at 805 ºC.